Advanced Powder Technology xxx (xxxx) xxx

Contents lists available at ScienceDirect

Advanced Powder Technology

journal homepage: www.elsevier.com/locate/apt

Original Research Paper

One-pot synthesis of isotype heterojunction g-C_3N_4-MU photocatalyst for effective tetracycline hydrochloride antibiotic and reactive orange 16 dye removal

Mochamad Solehudin [a], Uraiwan Sirimahachai [a,*], Gomaa A.M. Ali [b], Kwok Feng Chong [c], Sumpun Wongnawa [a]

[a] Department of Chemistry and Center of Excellence for Innovation in Chemistry, Faculty of Science, Prince of Songkla University, Hat Yai, Songkhla 90112, Thailand
[b] Chemistry Department, Faculty of Science, Al-Azhar University, 71524 Assiut, Egypt
[c] Faculty of Industrial Sciences & Technology, Universiti Malaysia Pahang, Gambang 26300, Kuantan, Malaysia

ARTICLE INFO

Article history:
Received 15 October 2019
Received in revised form 20 January 2020
Accepted 18 February 2020
Available online xxxx

Keywords:
g-C_3N_4
Heterojunction
Photocatalyst
Tetracycline hydrochloride
Reactive orange 16

ABSTRACT

The one-pot synthesis of g-C_3N_4-MU isotype heterojunction has been produced by the thermal polycondensation method by mixing different ratios of precursors between melamine and urea. The isotype heterojunction g-C_3N_4-MU samples were characterized by X-ray diffraction spectroscopy, scanning electron microscope and energy-dispersive X-ray-spectroscopy, UV–Visible diffuse reflectance spectroscopy, and X-ray photoelectron spectroscopy. The band-gap energy of these photocatalysts reveals that they can work well under visible light. The photocatalytic performance of the samples was investigated over the photodegradation of reactive orange-16 (RO-16) dye and tetracycline hydrochloride (TC-HCl) under visible light irradiation. The isotype heterojunction of g-C_3N_4-M6U10 showed the highest degradation of 95 and 85.6% for RO-16 and TC-HCl, respectively under irradiation time of 100 and 120 min. The major reactive species was identified as $\cdot O_2^-$. Moreover, the reusability of the photocatalyst was investigated up to 3 cycles with good efficiency. The present synthesized isotype heterojunction g-C_3N_4-MU could be applied as a facile pathway for synthesis and as an effective pathway to resolve various environmental problems.

1. Introduction

In recent decades, water pollution has emerged as one of the major threats in the world. The organic compounds such us reactive orange 16 dye (RO-16) and tetracycline hydrochloride (TC-HCl) have been widely used to fulfill human needs. However, both of them are poisonous and hazardous organic pollutants which if unconsciously discharged can pollute the environment, endangering the ecosystem and human health [1–3]. Consequently, it has become an imminent problem that must be addressed for the removal of organic pollutants from water [4–6].

The semiconductor photocatalysis has been considered as an efficient and attractive method for water pollutants separation, particularly organic pollutants degradation [7,8]. A graphitic carbon nitride (g-C_3N_4) has received great attention due to its matching band gap energy [9,10], high thermal and chemical stabilities [11], good electrical and optical properties [12], suitable electronic band structure and elemental abundance [13]. As such g-C_3N_4 is a very interesting material for photocatalytic application especially degradation of the pollutant [14,15]. A facile synthesis of g-C_3N_4 has been reported by thermal polycondensation of precursors using melamine, dicyanamide, thiourea, and urea [16–19].

Nevertheless, poor specific surface area and photo-absorption efficiency together with fast charge recombination of g-C_3N_4 become an obstacle to fully promote its photocatalytic activity [20,21]. To take better advantages of g-C_3N_4, there are various methods to modify the photocatalytic ability of g-C_3N_4 including metal/non-metal doping [22], metal deposition [23], constructed heterojunction [13], and copolymerization [24].

The band structure among semiconductors could be well-matched formation which can promote charge separation between the interface of two semiconductors [25]. The constructed heterojunction between suitable semiconductors is based on g-C_3N_4 with other materials, for example, TiO_2-g-C_3N_4 [20], BiOI-g-C_3N_4 [26], $BiVO_4$- g-C_3N_4 [27], $BiFeO_3$-g-C_3N_4 [28], CeO_2- g-C_3N_4 [29], etc.

* Corresponding author.
E-mail address: uraiwan.s@psu.ac.th (U. Sirimahachai).

https://doi.org/10.1016/j.apt.2020.02.020
0921-8831/

Furthermore, combining two semiconductors of g-C_3N_4 into the isotype heterojunction of g-C_3N_4 has been reported as an alternative pathway to resolve the limitation of g-C_3N_4. Isotype heterojunction of g-C_3N_4 prepared from thiourea and urea was able to promote the efficiency of electron-hole separation, thus improved the photocatalytic ability [30]. Likewise, isotype heterojunction of g-C_3N_4 prepared from cyanimide and urea could enhance photocatalytic performance due to the widening of band gap, more competitive CBM or VBM potentials, higher BET surface area, and thinner sheet morphology [31]. It is reported that isotype heterojunction of g-C_3N_4 prepared by dicyanamide-urea showed high photocatalytic performance [32]. Melamine and urea derived g-C_3N_4 were successfully prepared and showed improved photocatalytic activity [33]. These previous works have proven that combining two components of g-C_3N_4 precursors into isotype heterojunction of g-C_3N_4 can overcome the drawbacks and enhance the photocatalytic efficiency.

In this work, the isotype heterojunction of g-C_3N_4 -MU (MU = melamine and urea) was synthesized through thermal polycondensation employing melamine and urea as precursors. Urea, besides acts as a precursor, it could also be considered as a modifier or promoter to repair the deficiency of g-C_3N_4 as photocatalyst. Higher content of urea seems to affect the morphology into favoring more sheet-like which benefits the photocatalysis. The photocatalytic activity of g-C_3N_4-MU was investigated using RO-16 dye and TC-HCl under low energy (55 W Xe-lamp) visible light. The plausible photo-degradation mechanism was also proposed.

2. Experimental section

2.1. Materials

Melamine, urea (Sigma-Aldrich, USA); reactive orange 16 (RO-16) (Sigma-Aldrich, Germany); tetracycline hydrochloride (TC-HCl), isopropyl alcohol (Merck, Germany); ρ-benzoquinone (Sigma-Aldrich, China); and ethylenediaminetetraaceticacid (EDTA) (QreC, New Zealand) were of analytical grade. These materials were applied directly with no additional treatment.

2.2. Synthesis of g-C_3N_4-MU

The g-C_3N_4-MU samples were synthesized via a thermal-polycondensation method [18,32] by mixing melamine and urea precursors. Typically, the desired amounts of melamine (8 g) and urea (8 g) were combined by grinding in a mortar for 20 min. The obtained precursor powder was placed in the crucible with lid and heated to 550 °C for 2 h with a ramping rate of 5 °C min^{-1} under a normal atmosphere. Furthermore, the crucible was quenched to room temperature and the sample was reground to powder in a mortar. The obtained sample was assigned as *g-C_3N_4-M8U8*. Similarly, other samples were synthesized by tuning the precursor ratio with 10 g of melamine and 6 g of urea, 6 g of melamine and 10 g of urea and were denoted as g-C_3N_4-M10U6 and g-C_3N_4-M6U10, respectively. g-C_3N_4-M and g-C_3N_4-U also were prepared using 16 g of melamine alone and 16 g of urea alone, respectively, under the same conditions. The product yield of all samples was given in Table S1.

2.3. Characterizations

The phase structure of the sample was characterized by X-ray diffraction with Cu Kα radiation (XRD; Pert MPD, PHILIPS, the Netherlands). Chemical bonds and functional groups were characterized by FT-IR spectra acquired in the KBr pellet form (VERTEX 70, Bruker, Germany). The field emission scanning electron microscope (FE-SEM) with energy-dispersive X-ray spectrometry (EDS) was used to study the morphology of the samples. The N_2 adsorption-desorption isotherms were measured at −196 °C by N_2 adsorption system (ASAP2460, Micromeritics, USA) and the sample was degassed at 250 °C for 3 h before analysis. The specific surface area was calculated by the Brunauer-Emmett-Teller method (BET). X-ray photoelectron spectroscopy (XPS; AXIS Ultra DLD, Kratos Analytical Ltd) was used to analyze the surface chemical state. UV–Vis DRS (Shimadzu, UV-2450, Japan) was used to obtain the absorption spectra of samples in the reflectance mode in the range of 200–800 nm. The pH_{pzc} of samples was determined by Zeta potential analyzer (Model ZetaPALS, Brookhaven).

2.4. Electrochemical measurements

The electrochemical measurements were conducted by an electrochemical analyzer (AUTOLAB PGSTAT30, the Netherlands) with the standard three-electrode system. The sample was coated on the indium tin oxide (ITO) substrate and served as the working electrode. Pt wire was used as a counter electrode and Ag/AgCl as a reference electrode. The working electrodes were prepared by the following method: 4 mg of the prepared sample was dispersed into 1 mL ethanol and then ultrasonicated for 30 min. The suspension (20 μL) was drop-casted onto the ITO surface. KCl solution (0.2 mol L^{-1}) containing 5 mmol L^{-1} Fe $(CN)_6^{3-}/FeCN_6^{4-}$ was used as an electrolyte for the electrochemical impedance spectroscopy (EIS) investigation. The photocurrent test was measured under a 55 W Xenon Lamp and 0.5 mol L^{-1} Na_2SO_4 electrolyte solution.

2.5. Photocatalytic activity study

Photocatalytic study of all samples was conducted based on the efficiency of removal of organic compounds (RO-16 or TC-HCl) in an aqueous solution by dispersing the as-prepared g-C_3N_4-MU through the solution. A small amount of sample (150 mg) was discharged into 150 mL of an aqueous solution of organic compound (10 mg L^{-1} RO-16 or TC-HCl). The solution was then magnetically stirred under the dark for 30 min. to assure the adsorption/desorption equilibrium of dye onto the photocatalyst surface (Fig. S2). After that, the visible light (55 W Xe-lamp, HID, with a cutoff filter of 420 nm) was turned on. After irradiation at a pre-determined time, 3 mL of the organic solution was collected and centrifuged to separate the sample powders. The remaining organic compound was monitored by using UV–Vis spectrophotometer and determined the degraded products by liquid chromatography-mass spectra (ESI^- mode, Agilent Technologies, USA).

3. Results and discussion

3.1. Chemical structure and morphology characterization

3.1.1. XRD diffraction

The XRD diffraction of the obtained g-C_3N_4-M, g-C_3N_4-10M6U, g-C_3N_4-8M8U, g-C_3N_4-6M10U, and g-C_3N_4-U are given in Fig. 1a. The characteristic diffractions of all samples are the two consistent diffraction peaks which appear at around 13.0° and 27.0°, these two peaks can be indexed as (1 0 0) and (0 0 2) diffraction plane of g-C_3N_4 (JCPDS No.87-1526), respectively [33]. This could be used to confirm the existing of g-C_3N_4 [33–35]. The weak diffractions at around 13.0° of g-C_3N_4-M, g-C_3N_4-10M6U, g-C_3N_4-8M8U, g-C_3N_4- 6M10U, and g-C_3N_4-U are observed at 2θ angle of 12.57°, 12.88°, 12.73°, 12.86°, and 13.03°, respectively, corresponding to the triazine unit. It is noticed that (1 0 0) peak of isotype heterojunction samples are loacated between g-C_3N_4-M and g-C_3N_4-U,

Please cite this article as: M. Solehudin, U. Sirimahachai, G. A. M. Ali et al., One-pot synthesis of isotype heterojunction g-C_3N_4-MU photocatalyst for effective tetracycline hydrochloride antibiotic and reactive orange 16 dye removal, Advanced Powder Technology, https://doi.org/10.1016/j.apt.2020.02.020

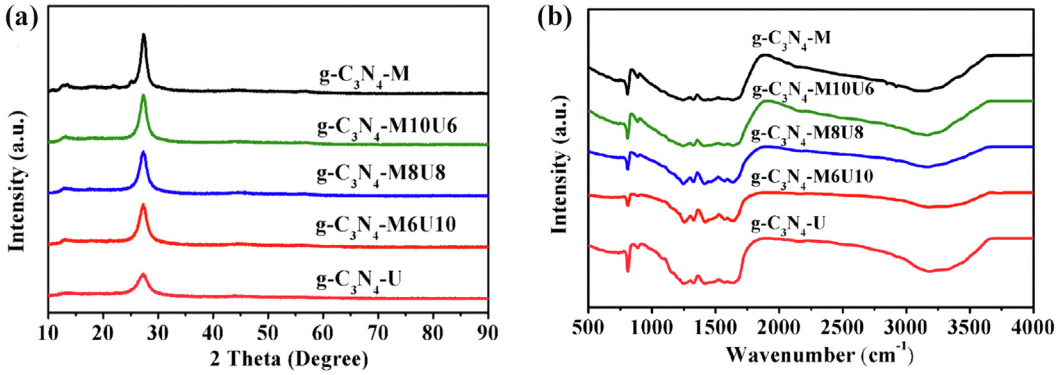

Fig. 1. XRD diffractograms (a) and FT-IR spectra (b) of the as-prepared photocatalysts.

implicating the formation of heterojunction among the samples. While the strong diffractions at around 27.0° are shifted to 27.32° for g-C_3N_4-M, 27.25° for g-C_3N_4-10M6U, 27.45° for g-C_3N_4-8M8U, 27.23° for g-C_3N_4-6M10U, and 27.33° for g-C_3N_4-U, corresponding to the interlayer stacking of the aromatic units of g-C_3N_4 [33,36]. These evidences support the success of synthesizing all these heterojunction compounds.

3.1.2. FT-IR spectra

Fig. 1b presents the FT-IR spectra of g-C_3N_4-M, g-C_3N_4-10M6U, g-C_3N_4-8M8U, g-C_3N_4-6M10U, and g-C_3N_4-U. The FT-IR spectra of all samples show similar absorption peaks at around 810 cm^{-1} which can be assigned to the breathing modes of triazine structure unit and sp^2 C = N [33,37]. Several absorption peaks in the region of 1200–1700 cm^{-1} can be assigned to the stretching vibration of C-N heterocyclic [33,37]. In addition, the broad absorption peaks from 3000 to 3400 cm^{-1} result from the stretching vibration of N-H bonds or NH_2 groups [33,37,38].

3.1.3. X-ray photoelectron spectroscopy

To recognize the chemical states of the samples, the XPS spectra were acquired and presented in Fig. 2. The survey spectra (Fig. 2a) reveal that all samples are composed of C and N as expected. The spectra of g-C_3N_4-M, g-C_3N_4-U, and g-C_3N_4-6M10U samples show that the binding energies of C1s and N1s core electrons are not significantly shifting which means that the chemical state of elements in the g-C_3N_4-6M10U are similar to those in the g-C_3N_4-M and g-C_3N_4-U. The C1s spectra in Fig. 2b reveal three major peaks at the binding energies around 288.5, 286.9, and 285 eV corresponding to C in the N—C=N, C—$(N)_3$, and sp^2 C=C bonds, respectively

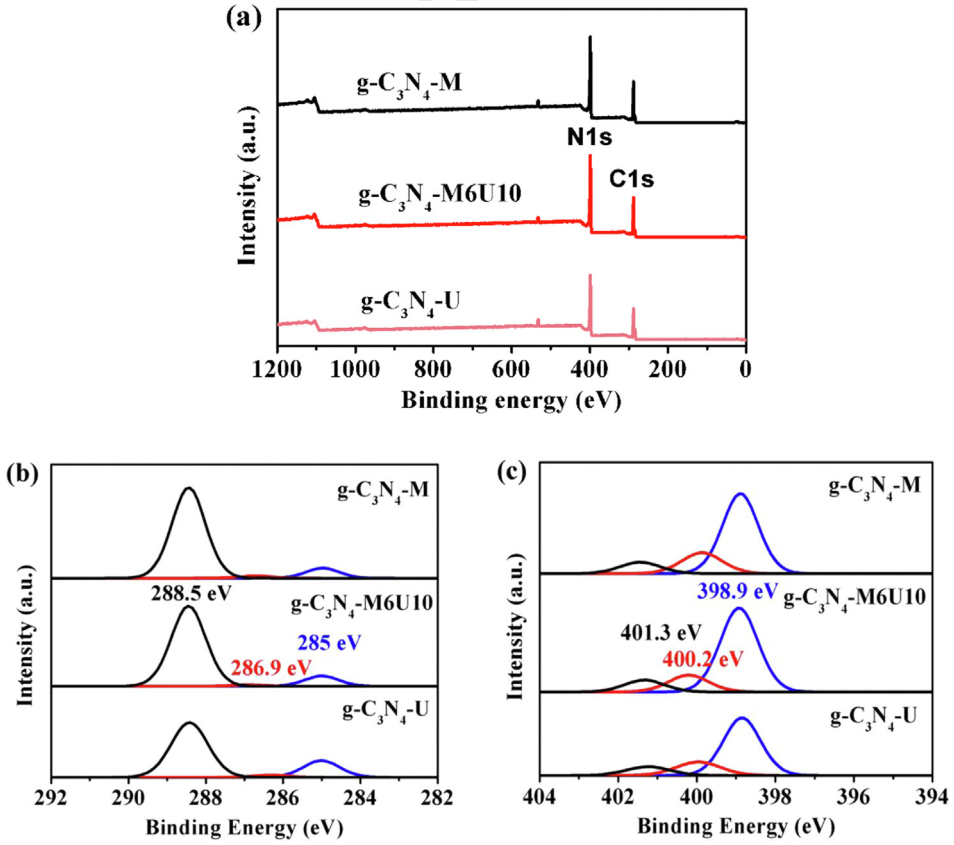

Fig. 2. XPS: survey (a), C1s (b), and N1s (c) spectra of synthesized g-C_3N_4-M, g-C_3N_4-M6U10, g-C_3N_4-U.

Please cite this article as: M. Solehudin, U. Sirimahachai, G. A. M. Ali et al., One-pot synthesis of isotype heterojunction g-C_3N_4-MU photocatalyst for effective tetracycline hydrochloride antibiotic and reactive orange 16 dye removal, Advanced Powder Technology, https://doi.org/10.1016/j.apt.2020.02.020

[30,39]. In Fig. 2c, the deconvoluted N1s spectra reveal three main peaks at around 398.9, 400.2, and 401.3 eV which can be assigned to C—N—C, N—(C)$_3$ groups, and amino function C-NH$_2$, respectively [39,40]. Based on the XRD, FT-IR, and XPS results suggest that isotype heterojunction of g-C_3N_4-MU has been completely synthesized.

3.1.4. The scanning electron microscopy

The detailed morphology study of all samples was performed by SEM and the elemental composition and distribution were also evaluated using EDS. The SEM images of g-C_3N_4-M, g-C_3N_4-10M6U, g-C_3N_4-8M8U, g-C_3N_4-6M10U, and g-C_3N_4-U are shown in Fig. 3. In Fig. 3a, g-C_3N_4-M is seen to compose of large solid bulk-like product and thick layers, meanwhile g-C_3N_4-U consists of sheets morphology with a high porosity on the surface of the sample (Fig. 3e). It can be clearly seen that g-C_3N_4-M and g-C_3N_4-U have different molecular structures that were mixed together as an isotype heterojunction. The resulting morphologies of the samples comprise of layers with different porosity (Fig. 3b–d). These results clearly indicate that g-C_3N_4-6M10U has a large number of pore on the surface than g-C_3N_4-10M6U and g-C_3N_4-8M8U. This is due to the higher content of urea in the molar ratio of isotype heterojunction, thus provide the larger number of pore structures leading to the larger specific surface area and plentiful reactive sites. This helps raise the photogenerated charge separation and may enhance the photocatalytic activity. In addition, the elemental analysis of the sample is confirmed in the EDS mapping spectra as shown in Fig. 3f. The elements of C and N are clearly seen with a uniform distribution over g-C_3N_4-6M10U with a percentage of 34.8 and 64.2% for C and N, respectively. Additionally, the presence of only C and N elements signify the purity of the samples.

3.1.5. Specific surface area

The measured specific surface area values are shown in Table 1. The g-C_3N_4-M has the lowest specific surface area of 4.69 m^2 g^{-1} whereas g-C_3N_4-U has the largest value of 36.55 m^2 g^{-1}. The speci-

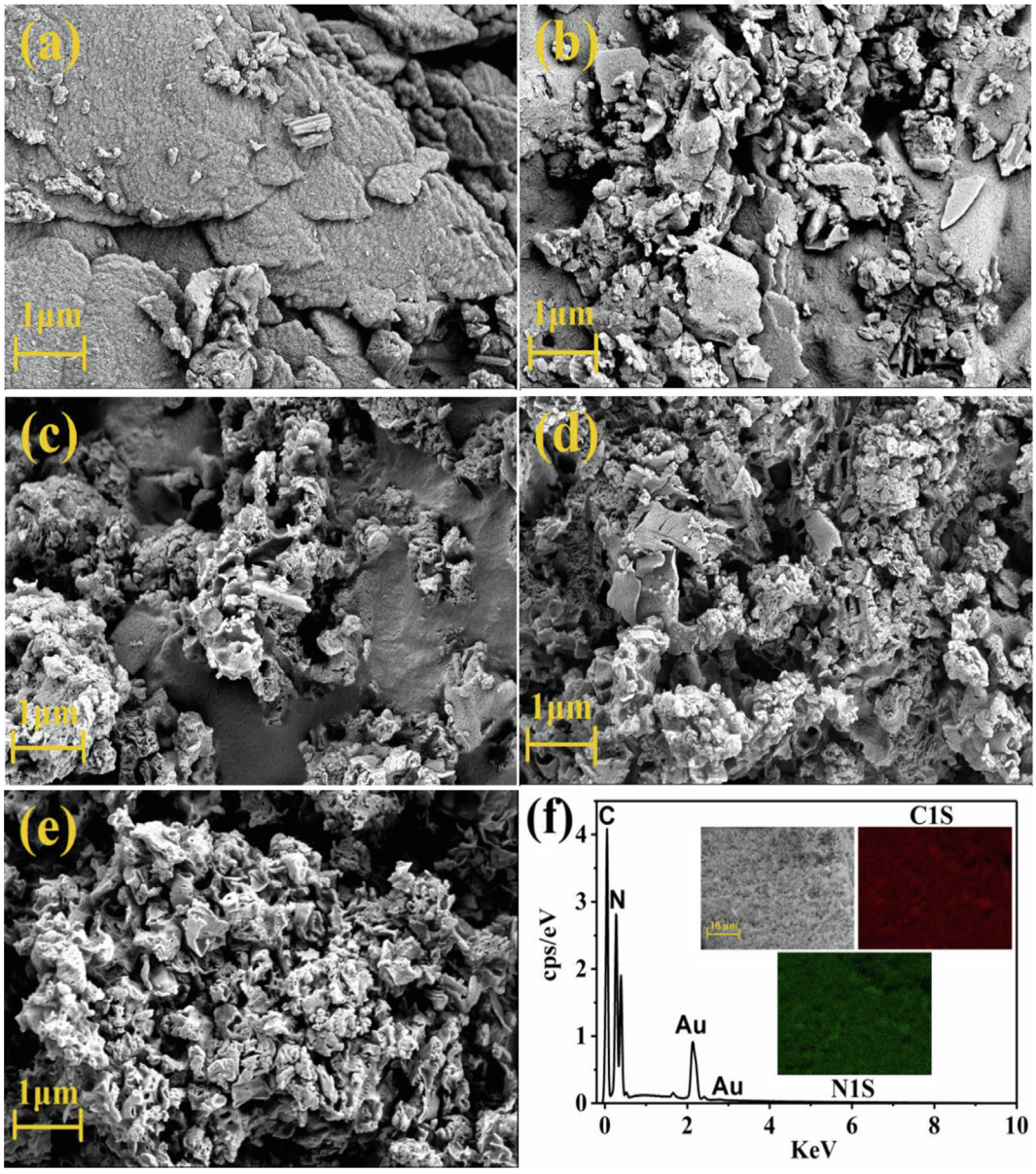

Fig. 3. SEM images (x 30,000) of as-prepared photocatalysts: g-C_3N_4-M (a), g-C_3N_4-M10U6 (b), g-C_3N_4-M8U8 (c), g-C_3N_4-M6U10 (d), g-C_3N_4-U (e), and EDS mapping spectra of g-C_3N_4-M6U10 (f).

Please cite this article as: M. Solehudin, U. Sirimahachai, G. A. M. Ali et al., One-pot synthesis of isotype heterojunction g-C_3N_4-MU photocatalyst for effective tetracycline hydrochloride antibiotic and reactive orange 16 dye removal, Advanced Powder Technology, https://doi.org/10.1016/j.apt.2020.02.020

fic surface areas of samples are significantly increased with increasing content of urea in the molar ratio of isotype heterojunction, e.g. 9.42, 10.09, and 15.87 $m^2 g^{-1}$ for g-C_3N_4-10M6U, g-C_3N_4-8M8U, and g-C_3N_4-6M10U, respectively. This trend consistent with the SEM results that the larger number of pore leads to the higher specific surface area which, in turn, one can expect more active species and higher reactivity to cause greater photocatalytic property of materials [32,41]. In this respect, the isotype heterojunction g-C_3N_4-6M10U was expected to exhibit the most enhanced photocatalytic degradation of organic compounds.

3.2. Optical and photoelectrochemical properties

3.2.1. Study of optical properties

UV–Vis diffused reflectance spectroscopy was studied to understand the optical properties of samples. As presented in Fig. 4a, g-C_3N_4-M, and g-C_3N_4-U show the absorption edge at around 450 and 440 nm, respectively. Meanwhile, the isotype heterojunction of g-C_3N_4-10M6U, g-C_3N_4-8M8U, and g-C_3N_4-6M10U exhibits the absorption edge at about 450, 448, and 445 nm, respectively. The band gap energy (Fig. 4b) of all samples was approximated by the Kubelka-Munk transformation using the plots of $(\alpha h\nu)^2$ versus photon energy [33,42]. The band gap energy was calculated as reported elsewhere [43] listed in Table 1. It can be described that the higher the amount of urea in mixed ratio leads to widening the band gap energy of photocatalyst which obstructs the electron-hole pairs recombination rate and causes greater performance in photocatalytic activity. The bandgap energies of isotype heterojunction samples are narrow in accordance with the optical absorption edge. The strong photo-response of isotype heterojunction samples in the UV–Vis region is believed to beneficially enhance photocatalytic activity [44].

Both optical absorption edge and band gap energy of mixed ratio photocatalysts fall in between those of g-C_3N_4-M and g-C_3N_4-U. This could be the result of a well-matched band structure of urea-derived g-C_3N_4 and melamine-derived g-C_3N_4 and offer a great potential design of g-C_3N_4-MU isotype heterojunction [25]. The band gap energies values have been estimated for g-C_3N_4-M, g-C_3N_4-M10U6, g-C_3N_4-M8U8, g-C_3N_4-M6U10, and g-C_3N_4-U and listed in Table 1. Attempt to locate the valence band (VB) and conduction band (CB) of the synthesized samples was carried out by using the following empirical equations [45];

$$VB = X + 0.5.E_g - E_o \quad (1)$$

$$CB = VB - E_g \quad (2)$$

where E_o is the energy of free electrons on the hydrogen scale (4.5 eV vs. NHE) and X is electronegativity of g-C_3N_4 (4.73 eV) [45]. The calculated VB values of 1.63, 1.64, 1.65, 1.66, and 1.69 eV were obtained for g-C_3N_4-M, g-C_3N_4-M10U6, g-C_3N_4-M8U8, g-C_3N_4-M6U10, and g-C_3N_4-U, respectively. Meanwhile, CB were estimated to be −1.17, −1.18, −1.19, −1.20, and −1,23 eV,

Table 1
BET specific surface area and band gap energy of all photocatalysts.

Samples	S_{BET} (m^2/g)	Band gap (eV)
g-C_3N_4-M	4.69	2.80
g-C_3N_4-M10U6	9.42	2.82
g-C_3N_4-M8U8	10.09	2.84
g-C_3N_4-M6U10	15.87	2.86
g-C_3N_4-U	36.55	2.93

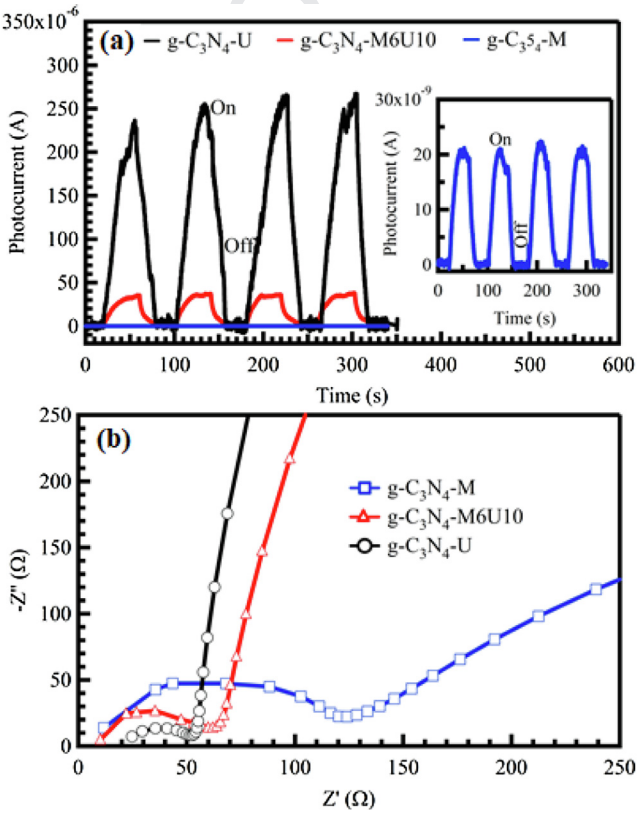

Fig. 5. (a) Photocurrents and Nyquist plots (b) of the synthesized g-C_3N_4-M, g-C_3N_4-M6U10 and g-C_3N_4-U. The inset of (a) shows an expanded scale of g-C_3N_4-M.

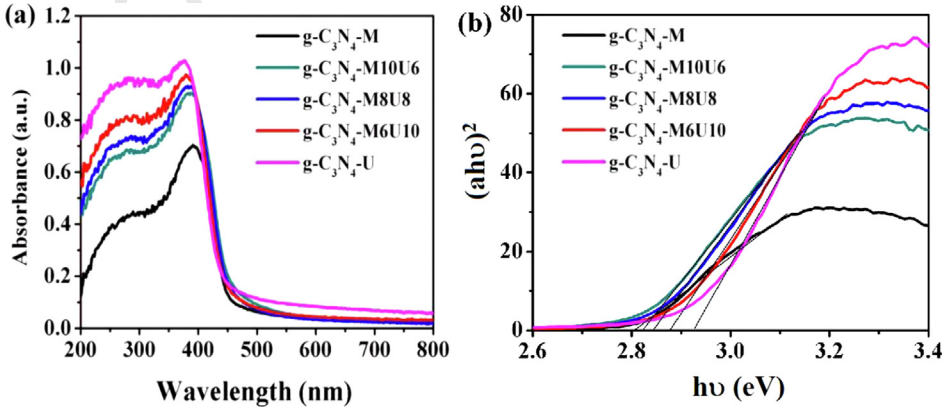

Fig. 4. UV–Vis DRS spectra (a) and band gap energy (b) of the synthesized photocatalysts.

Please cite this article as: M. Solehudin, U. Sirimahachai, G. A. M. Ali et al., One-pot synthesis of isotype heterojunction g-C_3N_4-MU photocatalyst for effective tetracycline hydrochloride antibiotic and reactive orange 16 dye removal, Advanced Powder Technology, https://doi.org/10.1016/j.apt.2020.02.020

respectively. Compared to g-C_3N_4-M, the g-C_3N_4-U and g-C_3N_4-M6U10 have larger band gap energy which provides a strong redox ability. As a result, the lifetime of charge carriers photoexcitation can be prolonged and improve its photocatalytic activity [39].

3.2.2. The photo-electrochemical properties

Chronoamperometry study (current vs. time) was performed to investigate the visible light response of the synthesized samples. The photo-electrochemical properties of g-C_3N_4-M, g-C_3N_4-M6U10, and g-C_3N_4-U were performed to observe the electron-holes separation efficiency in the samples. As shown in Fig. 5a, fast and uniform photocurrent responses were observed for all samples under visible light irradiation and such photoresponse was reversible. It is worth noting that the photocurrent response of g-C_3N_4-M6U10 isotype heterojunction was about 3.66×10^{-5} A which is higher than that in g-C_3N_4-M (2.11×10^{-8} A). Meanwhile, the photocurrent response of g-C_3N_4-U is the highest value (2.55×10^{-4} A). This indicates that g-C_3N_4-M indeed had the lowest photocurrent response owing to the fast charge recombination, while the photogenerated electron-hole pairs in the isotype heterojunction of g-C_3N_4-M6U10 were effectively separated due to the lower charge recombination. These observations were investigated by EIS experiments. The Nyquist curves of g-C_3N_4-M, g-C_3N_4-M6U10, and g-C_3N_4-U are depicted in Fig. 5b. The charge transfer resistance can be estimated from the radius of the extrapolated semi-circle at the high-frequency region and they are estimated to be 125.5 Ω, 51.6 Ω, and 35.1 Ω for g-C_3N_4-M, g-C_3N_4-M6U10, and g-C_3N_4-U, respectively. This small charge transfer resistance of g-C_3N_4-M6U10 indicates lower resistance for electron/hole to transfer across the electrode/electrolyte interface [46,47]. This consequence corroborates with the photocurrent result which confirmed that g-C_3N_4-U and g-C_3N_4-M6U10 were more effective in separate photo-induced charge carriers than that in g-C_3N_4-M. The high charge separation efficiency of samples could inhibit the rapid charge recombination, thus could be improved photocatalytic performance [39].

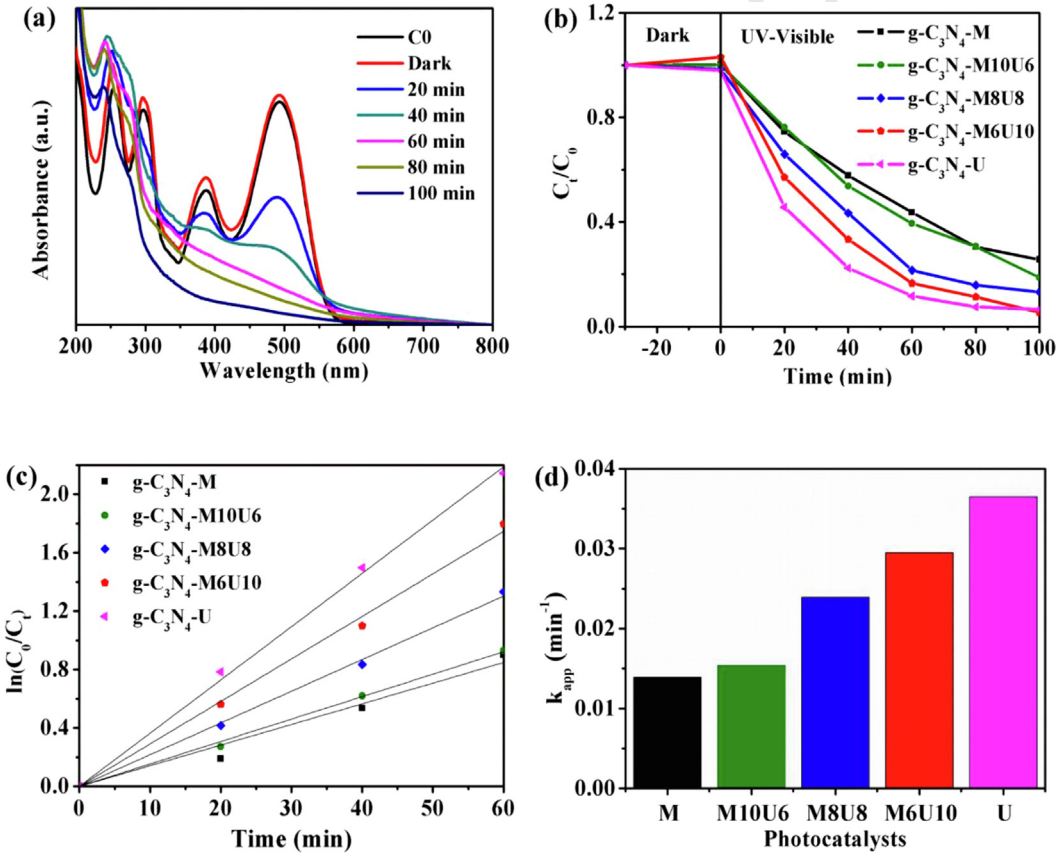

Fig. 6. Photocatalytic degradation of RO-16 dye (10 mg L^{-1}) under visible light irradiation: absorption of RO-16 dye (a), degradation rate (b), and kinetics rate over the synthesized photocatalysts (c-d).

Table 2
Photocatalytic degradation parameters of RO-16 and TC-HCl by the synthesized photocatalysts.

Photocatalysts	RO-16 (100 min)		TC-HCl (120 min)	
	Percent degradation (%)	k_{app} (min^{-1})	Percent degradation (%)	k_{app} (min^{-1})
g-C_3N_4-M	74.4	0.0139	70.6	0.0124
g-C_3N_4-M10U6	81.3	0.0154	71.1	0.0111
g-C_3N_4-M8U8	87.0	0.0217	73.1	0.0139
g-C_3N_4-M6U10	95.0	0.0295	85.6	0.0222
g-C_3N_4-U	93.4	0.0365	80.6	0.0190

Please cite this article as: M. Solehudin, U. Sirimahachai, G. A. M. Ali et al., One-pot synthesis of isotype heterojunction g-C_3N_4-MU photocatalyst for effective tetracycline hydrochloride antibiotic and reactive orange 16 dye removal, Advanced Powder Technology, https://doi.org/10.1016/j.apt.2020.02.020

3.3. The photocatalytic activity

The photocatalytic study was carried out for the degradation of RO-16 and TC-HCl under visible light. The absorption-desorption was allowed in the dark for 30 min.

3.3.1. The photocatalytic degradation of RO-16 dye

The RO-16 dye degradation was carried out for 100 min in the presence of the catalyst. The absorption of RO-16 at λ_{max} (493 nm, pH = 7) decreased with increasing reaction time. The RO-16 photodegradation performances of g-C_3N_4-M and g-C_3N_4-U are clearly different as shown in Fig. 6 that g-C_3N_4-U is more efficient than g-C_3N_4-M. In detail, g-C_3N_4-M and g-C_3N_4-U can degrade RO-16 74.4 and 93.4%, respectively, whereas the isotype heterojunction catalysts exhibit significantly greater photocatalytic performance than that of g-C_3N_4-M. The g-C_3N_4-M10U6, g-C_3N_4-M8U8, and g-C_3N_4-M6U10 achieve RO-16 dye degradation efficiency of 81.3, 87.0, and 95.0%, respectively. These isotype heterojunctions show greater photocatalytic activity than g-C_3N_4-M owing to their properties which have the larger specific surface area and higher porosity having abundant reactive sites as well as improving the electron-holes separation efficiency which can benefit to the photocatalytic activity improvement. The apparent rate constants were calculated as listed in Table 2. It could be seen that the photocatalytic rate of g-C_3N_4-M6U10 isotype heterojunction for degradation of R0-16 dye is much higher than other isotype heterojunction samples and g-C_3N_4-M, while the g-C_3N_4-U has the highest photocatalytic rate constant.

3.3.2. The photocatalytic degradation of TC-HCl

The degradation of TC-HCl was performed within 120 min in the presence of catalysts (Fig. 7). The maximum absorption wavelength (λ_{max}) of TC-HCl at pH = 7 appears at 360 nm. Similar to RO-16, the absorption spectra of TC-HCl decrease with the reaction time. Likewise, the isotype heterojunction samples show higher photocatalytic degradation of TC-HCl than that of g-C_3N_4-M, whereas g-C_3N_4-M6U10 shows the highest photodegradation rate of TC-HCl as shown in Table 2. It could be seen that the isotype heterojunction samples exhibit greater photocatalytic activity owing to assisted-urea composition which could make higher porosity and larger specific surface area in their photocatalyst properties as well as improving the electron-holes separation efficiency and then improved the photocatalytic activity. It can be assumed that in the case of urea addition as a precursor, urea can be modifier and promoter to repair the drawbacks of g-C_3N_4 as photocatalyst by using the isotype heterojunction of MU pathway.

3.3.3. The reusability and stability of photocatalyst

The reusability of the photocatalyst was evaluated using isotype heterojunction of g-C_3N_4-M10U6 for RO-16 dye and TC-HCl degradation as shown in Fig. 8a-b. The efficiency of RO-16 dye degradation was only slightly decreased while the degradation of TC-HCl significantly decreased after being reused for 3 times. Nevertheless, the lowest efficiencies (the 3th run) are still > 80% and > 60% for RO-16 and TC-HCl, respectively. Hence, the photocatalysts show good reusability in photocatalytic degradation. For the stability, the XRD spectra of isotype heterojunction of g-C_3N_4-M6U10

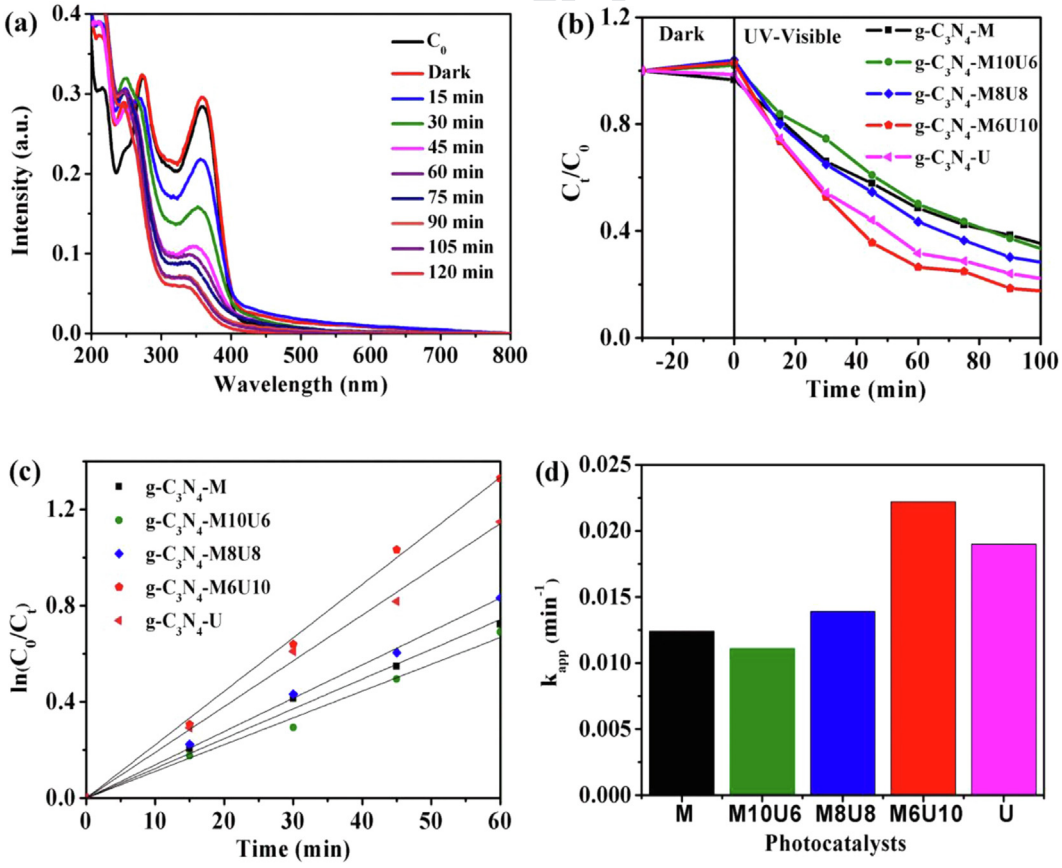

Fig. 7. Photocatalytic degradation of TC-HCl (10 mg L^{-1}) under visible light irradiation: adsorption of TC-HCl (a), degradation rate (b), and kinetics rate over the synthesized photocatalysts (c-d).

Please cite this article as: M. Solehudin, U. Sirimahachai, G. A. M. Ali et al., One-pot synthesis of isotype heterojunction g-C_3N_4-MU photocatalyst for effective tetracycline hydrochloride antibiotic and reactive orange 16 dye removal, Advanced Powder Technology, https://doi.org/10.1016/j.apt.2020.02.020

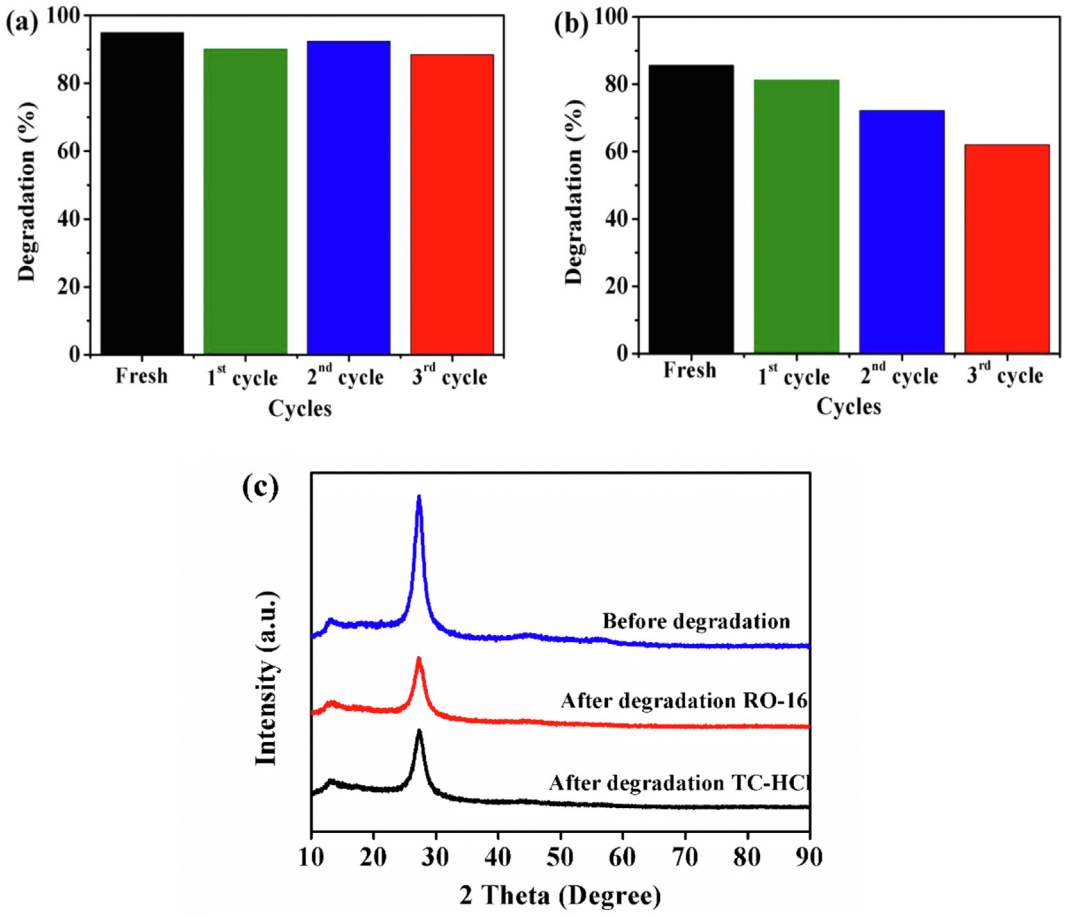

Fig. 8. The reusability and stability of g-C_3N_4-M6U10 photocatalyst; the repeated photocatalytic experiment for degradation RO-16 dye (a) and TC-HCl (b), and XRD diffractograms before and after degradation (c).

before and after the 3th run cycles are depicted in Fig. 8c which appears identical except slightly lower peak intensity after recycling reaction. It might be due to a narrowed interlayer stacking spaces of g-C_3N_4-M6U10 after 3 cycles [48].

3.3.4. Effect of initial pH on RO-16 dye and TC-HCl degradation

To study the initial pH effect on the degradation of RO-16 dye and TC-HCl, the experiments were carried out by varying the pH value from 3 to 11 over isotype heterojunction of g-C_3N_4-M6U10. The data of the initial pH effect on the RO-16 dye photodegradation are given in Fig. 9 a-b. In RO-16 solution at pH = 3, 5, and 7, the isotype heterojunction of g-C_3N_4-M6U10 can degrade 99, 98, and 95% RO-16 dye, respectively. In basic solution at pH 9 and 11, RO-16 showed lower degradation at 74 and 71%, respectively. With regard to the zeta potential (pH_{pzc}) of g-C_3N_4-M6U10 at pH 10.2, in acidic and neutral solution, the pH was lower than pH_{pzc} which caused the g-C_3N_4-M6U10 isotype heterojunction surface to be a positive charge, while in basic solution the surface of g-C_3N_4-M6U10 isotype heterojunction became negatively charged. Since the RO-16 dye was negatively charged [1], then it could be assumed that the positive charge of g-C_3N_4-M6U10 isotype heterojunction in the acidic medium has an electrostatic attraction which led to the strong adsorption between catalyst and RO-16 and resulted in great photodegradation efficiency. The negatively charged of g-C_3N_4-M6U10 isotype heterojunction in the basic medium has an electrostatic repulsion force with the negatively charged of RO-16 dye [49] forcing them apart, hence lower photodegradation performance.

Fig. 9 c-d, the photodegradation of TC-HCl under neutral pH 7 showed the maximum photodegradation rate. This can be explained by the pH related nature of TC-HCl as shown in Fig. 10 e, at pH = 7, the form of TC-HCl is neutral, but the surface charge of catalyst is positively charge (pH_{pzc} of g-C_3N_4-M6U10 = 10.2), hence the greater photodegradation of TC-HCl was obtained. In contrast, the strong repulsion between catalyst and TC-HCl occurred under both acidic and basic solution which led to lower photodegradation performance of TC-HCl. This repulsion arose from the positive surface charge of catalyst and the +1 charge of TC-HCl which occurred in acidic conditions. Likewise, in basic solution, the TC-HCl transformed into an anion ($-1/-2$) while the catalyst was deprotonated to be negatively charged.

3.3.5. The liquid chromatography-mass spectra analysis of organic compounds

The liquid chromatography-mass spectra analysis was further performed to identify the intermediate products of RO-16 dye and TC-HCl after photodegradation. The mass spectra of RO-16 dye and TC-HCl before and after the photocatalytic degradation process by g-C_3N_4-M6U10 are shown in Fig. 10. It can be seen that the RO-16 dye has been decomposed almost completely, and TC-HCl has been transformed into degraded products as detected in the mass spectra. In Fig. 10 a-b, the intermediate products of RO-16 dye with m/z = 474 (vinyl form) and 492 (hydrolyzed form) are other existing forms of RO-16 which are then photodegraded by the reactive species from the photocatalytic process to produce intermediate degraded products having m/z = 294, 284, and 201.

Please cite this article as: M. Solehudin, U. Sirimahachai, G. A. M. Ali et al., One-pot synthesis of isotype heterojunction g-C_3N_4-MU photocatalyst for effective tetracycline hydrochloride antibiotic and reactive orange 16 dye removal, Advanced Powder Technology, https://doi.org/10.1016/j.apt.2020.02.020

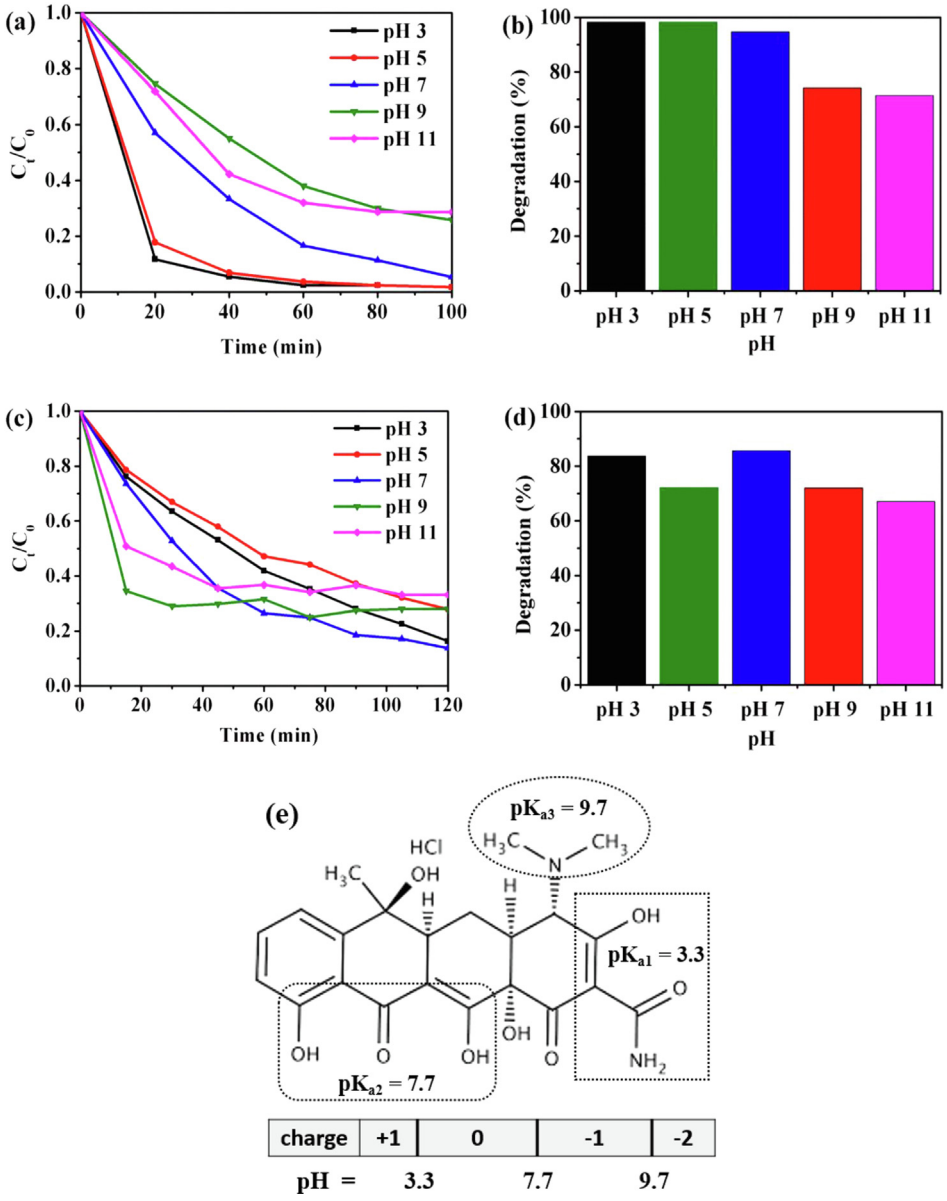

Fig. 9. The pH effect on photodegradation of RO-16 dye (a-b), TC-HCl (c-d) by g-C_3N_4-M6U10, and structure and pH-dependent specification of TC-HCl (e) [50].

The RO-16 dye and these degraded products are further decomposed and transformed into H_2O and CO_2 [51]. In Fig. 10 c, the m/z = 443 belongs to the TC-HCl which is further oxidized by the reactive species via the photodegradation to provides the degraded products with m/z ratio = 399, 325, 249, 180, and 135 (Fig. 10d). The TC-HCl and these degraded products are further decomposed and transformed into H_2O and CO_2.

3.4. The plausible photodegradation mechanism

The reactive species trapping experiment was investigated to identify reactive species for photodegradation of RO-16 dye and TC-HCl over isotype heterojunction g-C_3N_4-M6U10. Three typical scavengers, i.e. benzoquinone (BQ), isopropyl alcohol (IPA), and ammonium oxalate (AO) were applied on the RO-16 dye degradation as scavengers of $\cdot O_2^-$ (superoxide radical), $\cdot OH$ (hydroxyl radical), and h^+ (hole), respectively [7,52]. In the photodegradation of TC-HCl, three typical scavengers, i.e. BQ, IPA, and ethylenediaminetetraacetic acid (EDTA) were applied as scavengers of $\cdot O_2^-$, $\cdot OH$, and h^+ (hole), respectively [7,52,53]. As shown in Fig. 11a-b, the RO-16 dye degradation is clearly inhibited by BQ and slightly by AO, but IPA promoted the photocatalytic activity. As a result, the $\cdot O_2^-$ acts as the major and the $\cdot OH$ as the minor reactive species for RO-16 dye degradation.

Upon inspection Fig. 11c-d, the major reactive species of TC-HCl degradation is also $\cdot O_2^-$ with the $\cdot OH$ as a minor reactive species. Based on the result, the possible mechanism of RO-16 dye and TC-HCl degradation over isotype heterojunction of g-C_3N_4-M6U10 can be proposed in Fig. 12. After the visible light is exposed to the catalyst surface, the electron from VB of g-C_3N_4-M and g-C_3N_4-U will be photoexcited to CB due to the suitable band gap energy to produce electron-hole pairs. The electrons on the g-C_3N_4-U will be transferred to the g-C_3N_4-M because CB position of g-C_3N_4-U is more negative than that in g-C_3N_4-M. The electron on the CB of g-C_3N_4-M and g-C_3N_4-U, which are more negative than E (O_2/ $\cdot O_2^-$) (−0.33 eV), can easily reduce O_2 to produce $\cdot O_2^-$ [39,44]. However, the more negative VB position on the g-C_3N_4-M prohibits the holes on the g-C_3N_4-U to transfer to the g-C_3N_4-M. The photo-

Please cite this article as: M. Solehudin, U. Sirimahachai, G. A. M. Ali et al., One-pot synthesis of isotype heterojunction g-C_3N_4-MU photocatalyst for effective tetracycline hydrochloride antibiotic and reactive orange 16 dye removal, Advanced Powder Technology, https://doi.org/10.1016/j.apt.2020.02.020

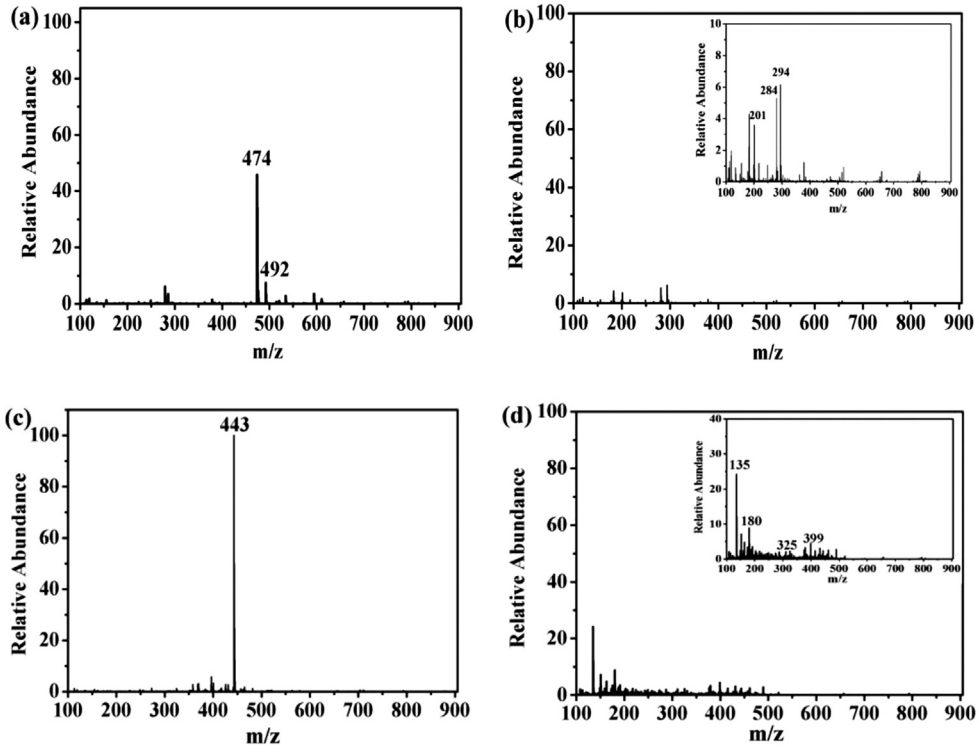

Fig. 10. Mass spectra of RO-16 dye before (0 min.) (a) and after photodegradation (100 min.) (b), and TC-HCl before (0 min.) (c) and after photodegradation (120 min.) (d) over g-C_3N_4-M6U10.

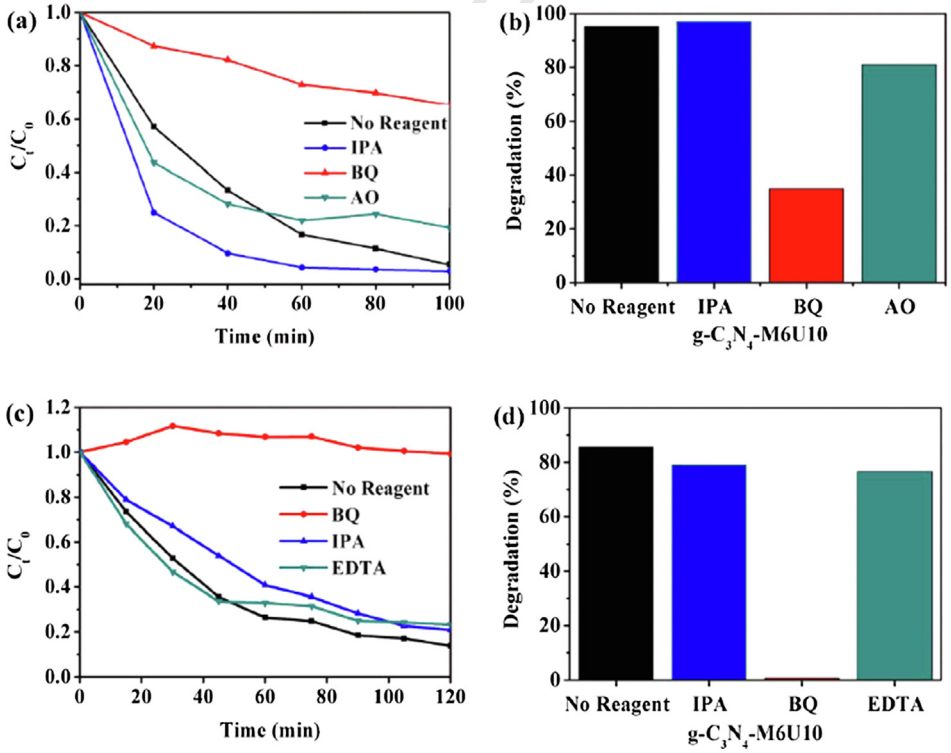

Fig. 11. Kinetic curves and degradation rates of RO-16 dye (a-b) and TC-HCl (c-d) over g-C_3N_4-M6U10 photocatalyst in the reactive species trapping experiments.

generated holes (h^+) in the VB of g-C_3N_4-M and g-C_3N_4-U can not produce ·OH because it is not positive enough to react with H_2O (E (·OH/OH^-) = (2.38 eV), but the holes can directly degrade the RO-16 dye and TC-HCl [39,44]. In conclusion, the $\cdot O_2^-$ (major reactive species) and h^+ (minor reactive species) attack the RO-16 dye (or TC-HCl) in solution to produce the degraded products which end as CO_2 and H_2O.

Please cite this article as: M. Solehudin, U. Sirimahachai, G. A. M. Ali et al., One-pot synthesis of isotype heterojunction g-C_3N_4-MU photocatalyst for effective tetracycline hydrochloride antibiotic and reactive orange 16 dye removal, Advanced Powder Technology, https://doi.org/10.1016/j.apt.2020.02.020

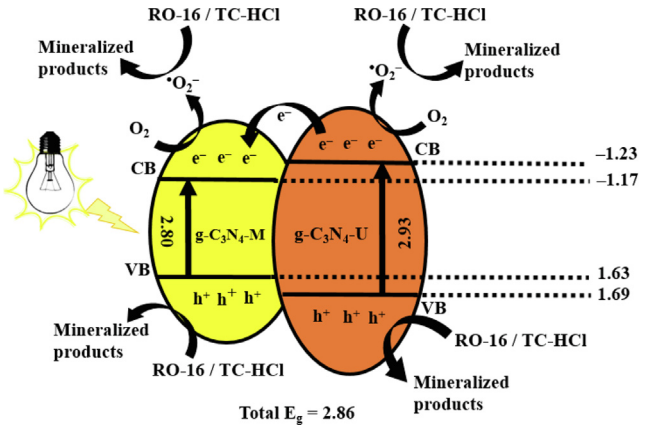

Fig. 12. The plausible photodegradation mechanism of RO-16 dye and TC-HCl over g-C_3N_4-M6U10 isotype heterojunction.

4. Conclusions

In summary, the isotype heterojunction of g-C_3N_4-MU was successfully synthesized from melamine and urea precursors. The product yield of all g-C_3N_4-MU samples are more than 7 times higher than g-C_3N_4-U. The content of urea in the mass ratio of g-C_3N_4-M6U10 isotype heterojunction can be as the modifier and promoter which improves the specific surface area and band gap energy, leads to the effective electron-hole separation, thus resulting in the enhanced photocatalytic degradation of RO-16 dye and TC-HCl. The photodegradation efficiency of RO-16 dye and TC-HCl was 95 and 85.6% within 100 and 120 min, respectively, under visible light irradiation. The $^{\cdot}O_2^-$ was the major reactive species in the RO-16 dye and TC-HCl photo-degradation, meanwhile the h^+ was minor reactive species which can directly degrade the RO-16 dye and TC-HCl. Therefore, the present method isotype heterojunction of g-C_3N_4-MU could be applied as a facile pathway for synthesis and as an effective process to resolve the problem of various environmental pollutants.

Acknowledgments

This work was supported by the Higher Education Research Promotion and Thailand's Education Hub for Southern Region of ASEAN Countries Project Office of the Higher Education Commission and Research Grant for Thesis Fiscal Year 2019, Graduate school, and the government budget of Prince of Songkla University (No. SCI6202067S), Faculty of Science, Prince of Songkla University, THAILAND. Financial support from the Center of Excellence for Innovation in Chemistry (PERCH-CIC), Ministry of Higher Education, Science Research and Innovation is also gratefully acknowledge. The researchers would like to thanks Asst. Prof. Dr. Warakorn Limbut for material supporting on electrochemistry experiments.

Appendix A. Supplementary material

Supplementary data to this article can be found online at https://doi.org/10.1016/j.apt.2020.02.020.

References

[1] A. Hayat, A. Elhassan, H. Abderrahim El, K. Kacem El, Electronic and optical properties of reactive orange 16 azo dye, Int. J. Innovation Appl. Stud. 8 (2014) 1447–1454.
[2] Y.Z. Hong, C.S. Li, G.Y. Zhang, Y.D. Meng, B.X. Yin, Y. Zhao, W.D. Shi, Efficient and stable Nb2O5 modified g-C_3N_4 photocatalyst for removal of antibiotic pollutant, Chem. Eng. J. 299 (2016) 74–84.
[3] A.S. Ethiraj, P. Uttam, V. K, K.F. Chong, G.A.M. Ali, Photocatalytic performance of a novel semiconductor nanocatalyst: Copper doped nickel oxide for phenol degradation, Mater. Chem. Phys. (2019), 122520.
[4] S.M. Seyed Arabi, R.S. Lalehloo, M.R.T.B. Olyai, G.A.M. Ali, H. Sadegh, Removal of congo red azo dye from aqueous solution by ZnO nanoparticles loaded on multiwall carbon nanotubes, Physica E 106 (2019) 150–155.
[5] A. Sharifi, L. Montazerghaem, A. Naeimi, A.R. Abhari, M. Vafaee, G.A.M. Ali, H. Sadegh, Investigation of photocatalytic behavior of modified ZnS:Mn/MWCNTs nanocomposite for organic pollutants effective photodegradation, J. Environ. Manage. 247 (2019) 624–632.
[6] H. Wongli, C.M. Goodwin, T.P. Beebe, S. Wongnawa, U. Sirimahachai, AgI-$BiYO_3$ photocatalyst: Synthesis, characterization, and its photocatalytic degradation of dye, Mater. Chem. Phys. 202 (2017) 120–126.
[7] Y. Hong, Y. Meng, G. Zhang, B. Yin, Y. Zhao, W. Shi, C. Li, Facile fabrication of stable metal-free CQDs/g-C_3N_4 heterojunctions with efficiently enhanced visible-light photocatalytic activity, Sep. Purif. Technol. 171 (2016) 229–237.
[8] S. Dyjak, W. Kicinski, A. Huczko, Thermite-driven melamine condensation to CxNyHz graphitic ternary polymers: towards an instant, large-scale synthesis of g-C_3N_4, J. Mater. Chem. A 3 (2015) 9621–9631.
[9] J. Zhu, P. Xiao, H. Li, S.A.C. Carabineiro, Graphitic carbon nitride: synthesis, properties, and applications in catalysis, ACS Appl. Mater. Interfaces 6 (2014) 16449–16465.
[10] C. Li, Y. Xu, W. Tu, G. Chen, R. Xu, Metal-free photocatalysts for various applications in energy conversion and environmental purification, Green Chem. 19 (2017) 882–899.
[11] P. Yang, H. Ou, Y. Fang, X. Wang, A facile steam reforming strategy to delaminate layered carbon nitride semiconductors for photoredox catalysis, 2017.
[12] Z. Yun, L. Lin, X. Ye, F. Guo, X. Wang, Helical graphitic carbon nitrides with photocatalytic and optical activities, 2014.
[13] T. Chen, C. Song, M. Fan, Y. Hong, B. Hu, L. Yu, W. Shi, In-situ fabrication of CuS/g-C_3N_4 nanocomposites with enhanced photocatalytic H2-production activity via photoinduced interfacial charge transfer, Int. J. Hydrogen Energy 42 (2017) 12210–12219.
[14] C. Zhou, C. Lai, D. Huang, G. Zeng, C. Zhang, M. Cheng, L. Hu, J. Wan, W. Xiong, M. Wen, X. Wen, L. Qin, Highly porous carbon nitride by supramolecular preassembly of monomers for photocatalytic removal of sulfamethazine under visible light driven, Appl. Catal. B 220 (2018) 202–210.
[15] X. Yuan, C. Zhou, Y. Jin, Q. Jing, Y. Yang, X. Shen, Q. Tang, Y. Mu, A.-K. Du, Facile synthesis of 3D porous thermally exfoliated g-C_3N_4 nanosheet with enhanced photocatalytic degradation of organic dye, J. Colloid Interface Sci. 468 (2016) 211–219.
[16] Y. Wang, Z. Wang, S. Muhammad, J. He, Graphite-like C_3N_4 hybridized $ZnWO_4$ nanorods: Synthesis and its enhanced photocatalysis in visible light, CrystEngComm 14 (2012) 5065–5070.
[17] J. Xu, H.-T. Wu, X. Wang, B. Xue, Y.-X. Li, Y. Cao, A new and environmentally benign precursor for the synthesis of mesoporous g-C_3N_4 with tunable surface area, PCCP 15 (2013) 4510–4517.
[18] W.-J. Ong, L.-L. Tan, Y.H. Ng, S.-T. Yong, S.-P. Chai, Graphitic carbon nitride (g-C_3N_4)-based photocatalysts for artificial photosynthesis and environmental remediation: Are we a step closer to achieving sustainability?, Chem Rev. 116 (2016) 7159–7329.
[19] F. Dong, Z. Wang, Y. Sun, W.-K. Ho, H. Zhang, Engineering the nanoarchitecture and texture of polymeric carbon nitride semiconductor for enhanced visible light photocatalytic activity, J. Colloid Interface Sci. 401 (2013) 70–79.
[20] H. Shao, X. Zhao, Y. Wang, R. Mao, Y. Wang, M. Qiao, S. Zhao, Y. Zhu, Synergetic activation of peroxymonosulfate by Co_3O_4 modified g-C_3N_4 for enhanced degradation of diclofenac sodium under visible light irradiation, Appl. Catal. B 218 (2017) 810–818.
[21] J. Zhang, Z. Ma, Porous g-C3N4 with enhanced adsorption and visible-light photocatalytic performance for removing aqueous dyes and tetracycline, hydrochloride (2018).
[22] G. Zhang, M. Zhang, X. Ye, X. Qiu, S. Lin, X. Wang, Iodine modified carbon nitride semiconductors as visible light photocatalysts for hydrogen evolution, Adv. Mater. 26 (2014) 805–809.
[23] L. Ge, C. Han, X. Xiao, L. Guo, In situ synthesis of cobalt–phosphate (Co–Pi) modified g-C_3N_4 photocatalysts with enhanced photocatalytic activities, Appl. Catal. B 142–143 (2013) 414–422.
[24] Z. Wang, Y. Huo, Y. Fan, R. Wu, H. Wu, F. Wang, X. Xu, Facile synthesis of carbon-rich g-C_3N_4 by copolymerization of urea and tetracyanoethylene for photocatalytic degradation of Orange II, J. Photochem. Photobiol., A 358 (2018) 61–69.
[25] H. Huang, S. Wang, Y. Zhang, P.K. Chu, Band gap engineering design for construction of energy-levels well-matched semiconductor heterojunction with enhanced visible-light-driven photocatalytic activity, RSC Adv. 4 (2014) 41219–41227.
[26] S.M. Aghdam, M. Haghighi, S. Allahyari, L. Yosefi, Precipitation dispersion of various ratios of BiOI/BiOCl nanocomposite over g-C3N4 for promoted visible light nanophotocatalyst used in removal of acid orange 7 from water, J. Photochem. Photobiol., A 338 (2017) 201–212.
[27] J. Zhao, J. Yan, H. Jia, S. Zhong, X. Zhang, L. Xu, $BiVO_4$/g-C_3N_4 composite visible-light photocatalyst for effective elimination of aqueous organic pollutants, J. Mol. Catal. A: Chem. 424 (2016) 162–170.

[28] T. Fan, C. Chen, Z. Tang, Y. Ni, C. Lu, Synthesis and characterization of g-C_3N_4/$BiFeO_3$ composites with an enhanced visible light photocatalytic activity, Mater. Sci. Semicond. Process. 40 (2015) 439–445.
[29] M. Li, L. Zhang, M. Wu, Y. Du, X. Fan, M. Wang, L. Zhang, Q. Kong, J. Shi, Mesostructured CeO_2/g-C_3N_4 nanocomposites: Remarkably enhanced photocatalytic activity for CO_2 reduction by mutual component activations, Nano Energy 19 (2016) 145–155.
[30] F. Dong, Z. Zhao, T. Xiong, Z. Ni, W. Zhang, Y. Sun, W.-K. Ho, In situ construction of g-C_3N_4/g-C_3N_4 metal-free heterojunction for enhanced visible-light photocatalysis, ACS Appl. Mater. Interfaces 5 (2013) 11392–11401.
[31] X. Fan, Z. Xing, Z. Shu, L. Zhang, L. Wang, J. Shi, Improved photocatalytic activity of g-C_3N_4 derived from cyanamide–urea solution, RSC Adv. 5 (2015) 8323–8328.
[32] F. Dong, Z. Ni, P. Li, Z. Wu, A general method for type I and type II g-C_3N_4/g-C_3N_4 metal-free isotype heterostructures with enhanced visible light photocatalysis, New J. Chem. 39 (2015) 4737–4744.
[33] I.M. Sundaram, S. Kalimuthu, P. Gomathi priya, Metal-free heterojunction of graphitic carbon nitride composite with superior and stable visible-light active photocatalysis, Mater. Chem. Phys. 204 (2018) 243–250.
[34] D.B. Hernández-Uresti, A. Vázquez, D. Sanchez-Martinez, S. Obregón, Performance of the polymeric g-C_3N_4 photocatalyst through the degradation of pharmaceutical pollutants under UV–vis irradiation, J. Photochem. Photobiol., A 324 (2016) 47–52.
[35] T. Muhmood, M.A. Khan, M. Xia, W. Lei, F. Wang, Y. Ouyang, Enhanced photo-electrochemical, photo-degradation and charge separation ability of graphitic carbon nitride (g-C_3N_4) by self-type metal free heterojunction formation for antibiotic degradation, J. Photochem. Photobiol., A 348 (2017) 118–124.
[36] S. Tan, Z. Xing, J. Zhang, Z. Li, X. Wu, J. Cui, J. Kuang, J. Yin, W. Zhou, Meso-g-C_3N_4/g-C_3N_4 nanosheets laminated homojunctions as efficient visible-light-driven photocatalysts, Int. J. Hydrogen Energy 42 (2017) 25969–25979.
[37] Z. Zhu, Z. Lu, X. Zhao, Y. Yan, W. Shi, D. Wang, L. Yang, X. Lin, Z. Hua, Y. Liu, Surface imprinting of a g-C_3N_4 photocatalyst for enhanced photocatalytic activity and selectivity towards photodegradation of 2-mercaptobenzothiazole, RSC Adv. 5 (2015) 40726–40736.
[38] H. Sadegh, G.A.M. Ali, S. Agarwal, V.K. Gupta, Surface Modification of MWCNTs with carboxylic-to-amine and their superb adsorption performance, Int. J. Environ. Res. 13 (2019) 523–531.
[39] Y. Shi, J. Huang, G. Zeng, W. Cheng, H. Yu, Y. Gu, L. Shi, K. Yi, Stable, metal-free, visible-light-driven photocatalyst for efficient removal of pollutants: Mechanism of action, J. Colloid Interface Sci. 531 (2018) 433–443.
[40] H. Wu, C. Li, H. Che, H. Hu, W. Hu, C. Liu, J. Ai, H. Dong, Decoration of mesoporous Co_3O_4 nanospheres assembled by monocrystal nanodots on g-C_3N_4 to construct Z-scheme system for improving photocatalytic performance, Appl. Surf. Sci. 440 (2018) 308–319.
[41] L. Jiang, X. Yuan, G. Zeng, X. Chen, Z. Wu, J. Liang, J. Zhang, H. Wang, H. Wang, Phosphorus- and sulfur-codoped g-C_3N_4: facile preparation, mechanism insight, and application as efficient photocatalyst for tetracycline and methyl orange degradation under visible light irradiation, ACS Sustainable Chem. Eng. 5 (2017) 5831–5841.
[42] E.A.A. Aboelazm, G.A.M. Ali, H. Algarni, K.F. Chong, Flakes size-dependent optical and electrochemical properties of MoS_2, Curr. Nanosci. 14 (2018) 1–5.
[43] G.A.M. Ali, O.A. Fouad, S.A. Makhlouf, Structural, optical and electrical properties of sol–gel prepared mesoporous Co_3O_4/SiO_2 nanocomposites, J. Alloy. Compd. 579 (2013) 606–611.
[44] L. Jiang, X. Yuan, G. Zeng, J. Liang, Z. Wu, H. Wang, J. Zhang, T. Xiong, H. Li, A facile band alignment of polymeric carbon nitride isotype heterojunctions for enhanced photocatalytic tetracycline degradation, Environ. Sci. Nano 5 (2018) 2604–2617.
[45] Y. Zheng, Z. Zhang, C. Li, A comparison of graphitic carbon nitrides synthesized from different precursors through pyrolysis, J. Photochem. Photobiol., A 332 (2017) 32–44.
[46] X. Wen, H. Zhang, Photoelectrochemical properties of CuS-GeO_2-TiO_2 composite coating electrode, PLoS ONE 11 (2016), e0152862.
[47] T. Dikici, S. Demirci, Influence of thermal oxidation temperature on the microstructure and photoelectrochemical properties of ZnO nanostructures fabricated on the zinc scraps, J. Alloy. Compd. 779 (2019) 752–761.
[48] Y. Wang, M. Qiao, J. Lv, G. Xu, Z. Zheng, X. Zhang, Y. Wu, g-C_3N_4/g-C_3N_4 isotype heterojunction as an efficient platform for direct photodegradation of antibiotic, Fullerenes, Nanotubes, Carbon Nanostruct. 26 (2018) 210–217.
[49] B. Viswanathan, Photocatalytic degradation of dyes: An overview, 2017.
[50] M. Liu, L.-A. Hou, S. Yu, B. Xi, Y. Zhao, X. Xia, MCM-41 impregnated with A zeolite precursor: Synthesis, characterization and tetracycline antibiotics removal from aqueous solution, Chem. Eng. J. 223 (2013) 678–687.
[51] Y. Wang, M. Qiao, J. Lv, G. Xu, Z. Zheng, X. Zhang, Y. Wu, g-C 3 N 4 /g-C 3 N 4 isotype heterojunction as an efficient platform for direct photodegradation of antibiotic, 2018.
[52] D. Pan, S. Ge, J. Zhao, Q. Shao, L. Guo, X. Zhang, J. Lin, G. Xu, Z. Guo, Synthesis, characterization and photocatalytic activity of mixed-metal oxides derived from NiCoFe ternary layered double hydroxides, Dalton Trans. 47 (2018) 9765–9778.
[53] M. Giahi, D. Pathania, S. Agarwal, G.A. Ali, K.F. Chong, V.K. Gupta, Preparation of Mg-doped TiO_2 nanoparticles for photocatalytic degradation of some organic pollutants, Stud. Univ. Babes-Bolyai, Chem. 64 (2019) 7–18.

Please cite this article as: M. Solehudin, U. Sirimahachai, G. A. M. Ali et al., One-pot synthesis of isotype heterojunction g-C_3N_4-MU photocatalyst for effective tetracycline hydrochloride antibiotic and reactive orange 16 dye removal, Advanced Powder Technology, https://doi.org/10.1016/j.apt.2020.02.020